Design of an instrumented microwave multimode cavity for sintering of nuclear ceramics

J. Croquesel, C. Meunier, C. Petit, F. Valdivieso, S. Pillon, A.C. Robisson, J. Martinez, F. Lemont

Materials and Design 204 (2021) 109638

Contents lists available at ScienceDirect

Materials and Design

journal homepage: www.elsevier.com/locate/matdes

Design of an instrumented microwave multimode cavity for sintering of nuclear ceramics

J. Croquesel [a,b], C. Meunier [a], C. Petit [a,*], F. Valdivieso [a], S. Pillon [b], A.C. Robisson [b], J. Martinez [c], F. Lemont [c]

[a] Mines Saint-Etienne, Université Lyon, CNRS, UMR 5307 LGF, Centre SMS, F-42023 Saint-Etienne, France
[b] CEA/DES/IRESNE/DEC/SETC, Centre de Cadarache, 13115 Saint-Paul-lez-Durance, France
[c] CEA/DES/ISEC/DMRC/STDC/LRVE, Centre de Marcoule, BP17171, 30207 Bagnols sur Cèze, France

HIGHLIGHTS

- New multimode microwave cavity and sintering cell for sintering of nuclear ceramics, designed by Finite Element simulation.
- Automated and instrumented setup for direct and reliable comparison with conventional sintering.
- Stable and homogeneous microwave heating of nuclear ceramics under reducing atmosphere.
- Sintering of dense UO2 crack free pellets with a shorter sintering cycle (4 h) than under conventional sintering (24 h).

GRAPHICAL ABSTRACT

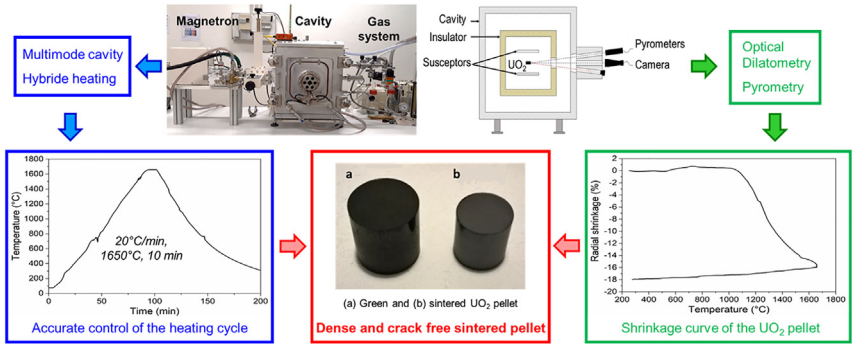

ARTICLE INFO

Article history:
Received 11 November 2020
Received in revised form 3 March 2021
Accepted 5 March 2021
Available online 8 March 2021

Keywords:
Microwave sintering
Nuclear fuel
Finite elements

ABSTRACT

This paper describes the development of an innovative instrumented and automated 2.45GHz multimode microwave cavity for sintering of uranium oxide based nuclear fuels (UO_2, $(U,Pu)O_2$, $(U,Am)O_2$ …). The cavity and the sintering cell were designed using Finite Element simulation and the expertise acquired over years on microwave heating. This original setup allows for hybrid and homogeneous heating of nuclear fuels. Reliable *in situ* monitoring of the samples' shrinkage and temperature is performed with an optical dilatometer and infrared pyrometers calibrated with a specific protocol. A dedicated software including a Proportional-Integral-Derivative (PID) controller was developed to precisely control the sintering cycles like under conventional heating. The setup is also designed for operating in a glovebox under reducing sintering atmosphere.

A stable and homogeneous heating with controlled sintering cycles is reached to successfully sinter UO_2 crack free pellets to high density. This is a key point of innovation compared to previous studies in the literature on microwave sintering of nuclear ceramics. The pellets' final densities are equivalent to those obtained under conventional sintering, but with a significant decrease in the total duration of the sintering cycle.

1. Introduction

Microwave sintering was deeply studied in the last decades due to its potential advantages compared to conventional heating [1,2]. Studies on various ceramics (*e.g.*, alumina, zirconia, hydroxyapatite) have shown densification of fine-grained samples with reduced processing times compared to conventional sintering [3–5]. These benefits are related to the heating process: the electromagnetic field directly heats the samples by dipolar polarization, leading to higher heating rates and lower dwell times [6]. Therefore, microwave sintering has a potential economic and environmental interest, especially for ceramics which

* Corresponding author.
E-mail address: clemence.petit@mines-stetienne.fr (C. Petit).

https://doi.org/10.1016/j.matdes.2021.109638

require a long sintering time like nuclear fuels. Nuclear ceramics are generally prepared by the conventional metallurgical powder process with the following steps: preparation of powder, milling, pressing into green pellets and sintering. This last step is carried out at a temperature range of 1650–1750 °C with a minimum dwell time of 4 h under reducing atmosphere (generally Ar/H_2) [7,8]. Few studies have reported densification of UO_2 by microwave sintering. Ford *et al.* succeeded in heating in few minutes UO_2 pellets until 1100 °C [9]. Subramanian *et al.* achieved a relative density of 95.5% Theoretical Density (TD) within a sintering time of less than 1 h [10]. Yang *et al.* attempted to sinter the specimens at heating rates of 20–30 °C/min but they noted formation of cracks [11]. Despite promising results, these investigations showed the difficulty to obtain defect-free samples and to precisely control heating cycles. This problem has also been encountered for microwave sintering of other ceramics [12,13] and is mainly due to the use of thermocouples for temperature measurement. The reliability of a thermocouple is low because it generally interacts with the electromagnetic field and gives a wrong measurement of the temperature. Moreover, thermocouples can disturb the field in the vicinity of the samples and induce heterogeneous heating of ceramic parts. It is necessary to use specific temperature measurement methods to precisely control and follow up the microwave sintering. Pert *et al.* first proposed to use pyrometers as a contactless temperature measurement technique [14]. Similarly, contactless dilatometric methods have been set up to measure the samples' shrinkage [15,16].

Another characteristic of microwave heating is the volumetric heating of materials. Unlike conventional solutions, where heat is transferred by convection or conduction from the outside to the product through its surface, microwaves heat the entire product mass directly and homogeneously. However, interaction of ceramics with microwaves depends on the material's dielectric properties. Some ceramics (*e.g.*, alumina) have a low dielectric loss tangent at low temperature and a coupling susceptor (*i.e.*, a material having high dielectric loss at room temperature) can be required to initiate heating. The effect of this susceptor (nature, geometry, relative position to the sample) on the electromagnetic field distribution in the cavity has to be taken into account [17].

Moreover, sintering of nuclear pellets in a microwave cavity requires to take into account different specifications: high sintering temperatures, control of the atmosphere during the thermal treatment and possibility to use the cavity in a glove box (for radiological protection).

For these reasons, a complete study on microwave sintering of nuclear fuels firstly necessitates to design a specific microwave cavity. Such an experimental setup was developed and is described in this paper. A particular attention was paid to the dimensions and geometries of the cavity and the sintering cell (*i.e.*, the insulation box which contains the specimen to heat and the susceptors). Both were designed using Finite Element (FE) simulation to optimize the electromagnetic field distribution in susceptors and samples. Reliable *in situ* monitoring of the samples' shrinkage and temperature is performed with an optical dilatometer and calibrated pyrometers. Temperature measurement by pyrometers is also used by a dedicated software, including a PID controller, which automatically modifies the microwave power in the cavity to precisely control sintering cycles. A detailed description of the whole setup is given in this paper. Results of UO_2 pellets sintering are also presented to demonstrate the ability of the setup to sinter nuclear fuels but also the accuracy of dilatometric measurements and control of thermal cycles.

2. The microwave setup

2.1. Main elements of the setup

The microwave furnace designed in this study is a 2.45 GHz multimode parallelepipedic cavity equipped with standard elements of a microwave setup (Fig. 1). Microwaves are produced by a magnetron powered with a 3 kW generator (*GMP 30KSM 56 T208 FST 3 IR, Sairem, France*). Power sensors are placed between the magnetron and the cavity to measure the incoming power inside the cavity and the outgoing reflected power from the cavity. These incident and reflected powers are continuously measured during sintering to precisely control heating cycles (see part 2.3.3). A standard WR340 waveguide with a TE10 propagation mode is used to transfer microwaves from the magnetron to the cavity. This waveguide is equipped with an impedance tuner (*AI EH WR340, Sairem, France*) which aims at minimizing the reflected power outgoing from the cavity, *i.e.* at maximizing the power transmission from the source (magnetron) to the load in the cavity. A mode stirrer, made of copper blades (for its high electrical conductivity), is used inside the cavity to obtain a homogeneous heating and to limit hot spots. To use this setup in a glovebox, the surface temperature of the cavity must remain under 50 °C to avoid melting of the gloves. For this purpose, the walls of the cavity are equipped with a water cooling system designed with copper tubes for efficient transfer of calories (Fig. 1). Moreover, the cavity is equipped with a sliding door and specific lockers to facilitate its use inside the glovebox (Fig. 1). A gas system is also used to control the sintering atmosphere with Ar/H_2 and the cavity is sealed to allow for a slight Ar/H_2 overpressure during sintering of samples.

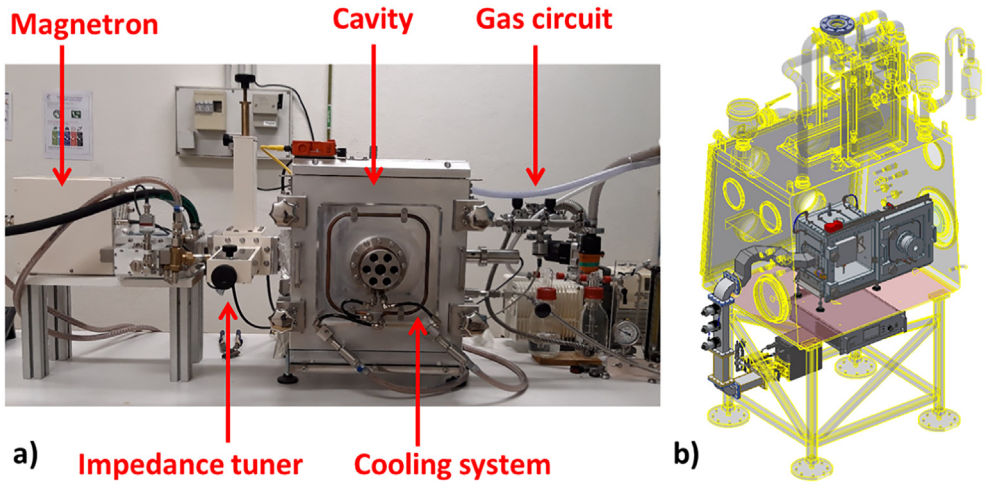

Fig. 1. a) Picture showing the main standard elements of the setup and b) drawing showing its integration in a glove box.

Internal sizes of the multimode cavity are important parameters to optimize the sample heating. According to previous work [18], internal sizes were chosen to be close to $n\lambda/2$ (with n being an integer and λ the wavelength corresponding to the frequency of the magnetron) to obtain a homogeneous distribution of the field inside the cavity. In order to get the highest field intensity at the cavity center, n was chosen to be an odd number. Moreover, the cavity sizes must be determined considering also the size and the properties (permittivity and electrical conductivity) of the components constituting the sintering cell (see part 2.2). Furthermore, sizes of the microwave furnace are also limited by the depth and height of the glovebox (around 800 mm). Taking all these conditions into account, FE simulations were carried out with COMSOL Multiphysics software (Electromagnetic Wave module) to calculate the internal sizes of the cavity (close to $n\lambda/2$), with n an odd number and $n\lambda/2 < 800$ mm.

Chimneys are used to measure temperature (pyrometers) and shrinkage (optical dilatometry) of the UO_2 sample during sintering (see part 2.3 and Fig. 3). Chimneys dimensions were also determined by FE simulation (not shown here) to prevent from electromagnetic leakage outwards.

2.2. The sintering cell

The sintering cell developed for heating of nuclear ceramics is made of thermal insulators and susceptors. Thermal insulators are made of aluminosilicate fibers plates (KVS 184–400, *Rath®, Germany*) to minimize heat losses from the sample and the susceptors by conduction and radiation. The *Rath®* material is used because it follows the main requirements for microwave applications: transparency to microwaves, stability at high temperature (until 1800 °C) and low thermal conductivity (0.33 $W.m^{-1}.K^{-1}$ at 1400 °C). External dimensions of the cell were chosen in accordance with the internal dimensions of the cavity and close to $n'\lambda/2$, with n' an odd number. This design limits the creation of reflected waves on the crucible surface which could be in phase opposition with incident waves (otherwise, the total wave would be cancelled).

UO_2 properties change with temperature, including the electrical conductivity which increases above 1300 °C [19]. Increase of the electrical conductivity has a strong impact on the penetration depth of the field inside UO_2 ([19,20] penetration depth decreases with the electrical conductivity). Due to this effect, less energy is dissipated in UO_2 at sintering temperatures and it is difficult to keep a high and constant heating rate of the sample (>10 °C/min), unless using high power levels (limited to 3 kW with the generator). To get around this problem, susceptors are used in the sintering cell to provide complementary thermal energy (mainly by radiation) to the sample in order to keep high and constant heating rates. Moreover, the use of susceptors allows for a hybrid and uniform heating through the entire sintering process. FE simulation (COMSOL - Electromagnetic Waves module) was used to determine the appropriate dimensions and positions of these susceptors inside the sintering cell and the furnace. In the simulation, cavity boundaries were considered as perfect electric conductors and the incoming power in the cavity was set to a constant value of 500 W. Inside of the cavity was considered as air with a relative permittivity $\varepsilon = 1$. The *Rath®* material used as insulator for the sintering cell was considered as perfectly transparent to microwaves and not taken into account in FE simulation. Only the UO_2 sample (cylindrical pellet 10 mm height and 8 mm diameter) and the susceptors were simulated in the cavity. Silicon carbide and 3Y-TZP (3 mol% yttria stabilized zirconia) were selected for the nature of the susceptors because they are frequently used for this application due to their interesting dielectric properties (high permittivity and low electrical conductivity) [17]. Table 1 shows the values of real and imaginary parts of permittivity (values at room temperature) used in the FE calculations for UO_2, SiC and 3Y-TZP [17,21,22]. Dielectric properties of UO_2 are poorly known and few values are available in the literature. The real part of the permittivity of UO_2 given by Gesi *et al.* [21] at 9.4GHz was used for the calculations and assumed to be equivalent at 2.45GHz. The imaginary part of the permittivity was set to $\varepsilon'' = 0.4$ because we hypothesize a similar heating behavior of UO_2 and SiC under microwave heating.

Table 1
Material data for FE simulation.

	UO_2	SiC	3Y-TZP
Real part of permittivity ε'	22	10	18
Imaginary part of permittivity ε''	0.4	0.4	0.04
Electrical conductivity σ (S/m)	10^{-3}	10^{-5}	10^{-9}

Fig. 2 shows the results of the electric field distribution inside the cavity with the optimized configuration of the susceptors (size, geometry and position). The electric field concentrates mainly in and around the susceptors / UO_2 pellet. The field penetrates inside each susceptor plate, whether for SiC (Fig. 2.a) or 3Y-TZP (Fig. 2.b) and the average electric field is equivalent in the lower and the upper plate (see Table 2), because the same field pattern is calculated. This effect will enable for equivalent heating of both plates and will lead to homogeneous heating of the UO_2 sample by susceptors.

However, the average electric field is more uniform and of higher intensity in 3Y-TZP susceptors than in SiC (see Fig. 2 and Table 2), due to the higher imaginary part of the permittivity of 3Y-TZP and its lower electrical conductivity (see Table 1).

Table 2 indicates that the average electric field in the UO_2 pellet is lower than in the susceptors. Despite this effect, the higher permittivity of UO_2 will allow for direct heating by the field. However, the average electric field in the UO_2 pellet is higher using 3Y-TZP susceptors than SiC. This effect, combined with the higher average electric field in 3Y-TZP susceptors compared to SiC, demonstrates that the use of 3Y-TZP should be of better interest to limit the power needed to heat the UO_2 sample.

To conclude, FE simulations demonstrate that the arrangement of the susceptors in the cell enables for hybrid heating of the pellet. No "screening effect" of the susceptors or the UO_2 sample occurs with this arrangement, whatever the nature of susceptors. SiC and 3Y-TZP are both of interest but the use of 3Y-TZP could limit the power needed to heat and sinter UO_2 sample. The less the power inside the cavity, the less the probability to create hot spots, arcing or plasma when sintering at high temperatures under reducing atmosphere.

2.3. Control and monitoring of the sintering

2.3.1. Optical dilatometry

Optical dilatometry is used to record the shrinkage of the samples during sintering. This technique was developed in previous studies [15,16]. A CCD camera (*RT-mvBC-X104iG, Opto Engineering, Italy*) records pictures of the flat circular face of the cylindrical sample through a chimney and a hole in the sintering cell (see Fig. 3a and 3b). A low-pass filter (filtering wavelengths higher than 700 nm) and a band pass filter (600–650 nm) are used to select only the wavelength range for which the camera lens is optimized. Filters also reduce chromatic aberrations, which can lead to errors in the sample diameter measurement. The camera is placed face to the central chimney with a specific support designed to precisely adjust it (see Fig. 3a and 3b). Three LEDs (*CREE XREWHT-L1–0000-009E7, Conrad, France*) are placed on two other chimneys to light the sample at low temperature. For high temperatures (>700 °C), the sample is visible due to its own radiation. Recorded images are processed after sintering with a home-made Labview® software (*National Instruments, USA*) which automatically detects pellet's edges, to measure its diameter [15,16]. The program finally output the evolution of the pellet diameter during sintering.

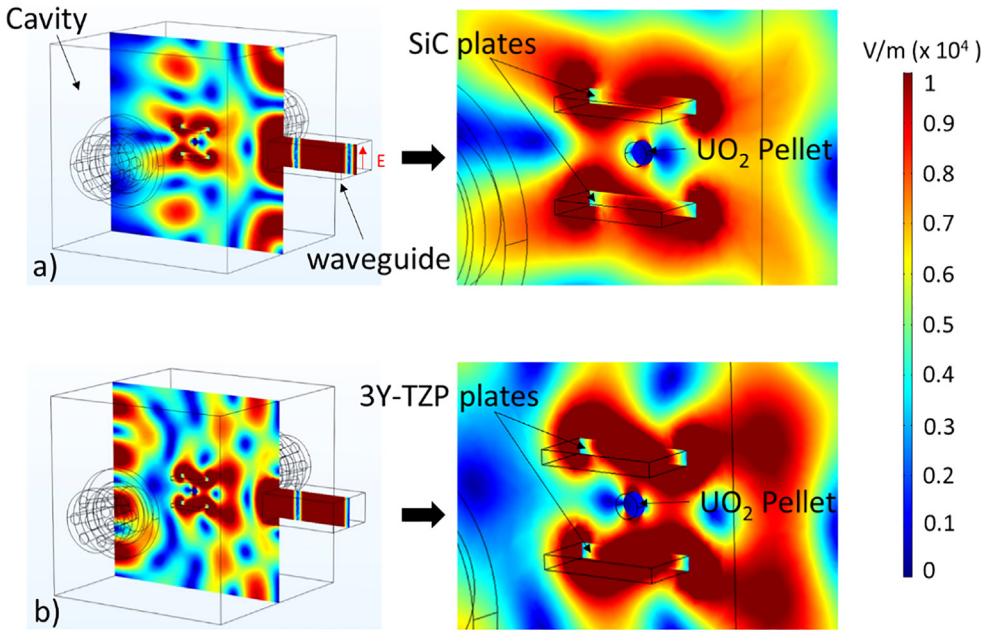

Fig. 2. Computed electric field pattern in the furnace with a) two SiC plates in horizontal position and b) two 3Y-TZP plates in horizontal position.

Table 2
Average electric field norm inside the UO_2 pellet and the SiC and 3Y-TZP susceptors calculated for an input power of 500 W in the cavity.

	Electric field norm (V/m)	
	SiC susceptors	3Y-TZP susceptors
Susceptor plate above UO_2 pellet	6326	7483
Susceptor plate below UO_2 pellet	6333	7479
UO_2 pellet	781	1005

2.3.2. Temperature measurement

Temperature measurement is performed with IR pyrometers. Due to the large temperature range to cover (from room temperature to 1700 °C), two pyrometers are used: a monochromatic pyrometer sensitive to wavelengths 2–2.5 μm in the temperature range 75–1300 °C (*IGA6/23, Lumasense Technologies, Germany*) and a bichromatic pyrometer sensitive to wavelengths 0.9–1.05 μm in the temperature range 700–1800 °C and equipped with a thermal camera (*ISR6-TI, Lumasense Technologies, Germany*). Pyrometers are focused on the flat circular face of the UO_2 pellet through chimneys and the hole in the sintering cell and precisely arranged using the same support as the camera (see Fig. 3). To get an accurate measurement with pyrometers, it is necessary to know the apparent emissivity ε of UO_2 in the experimental conditions, which depends on the sample surface (nature, roughness…) and its environment (susceptors and insulator material). A calibration protocol of the apparent emissivity, based on the melting point of selected oxide materials, was used to determine ε in the real sintering conditions. A detailed description of this protocol can be found elsewhere [16,23]. Briefly, a small amount of oxide powder with a known melting point was inserted in the hole of a UO_2 annular pellet (diameter of 9.6 mm, height of around 13 mm and hole diameter of 2.6 mm). The pellet was slowly microwave heated (< 5 °C/min) in the sintering cell until the melting of the oxide (detected with the camera). When the oxide started to melt, the emissivity of the pyrometers was modified to match the pellet temperature with that of the oxide melting temperature. Two oxides were used according to their melting temperature and stability at high temperature: GeO_2 with a melting temperature of 1115 °C, (*Puratronic, Alfa Aesar*) and Nb_2O_5 with a melting temperature of 1512 °C (*HC-Starck*). Three calibration tests for each oxide were

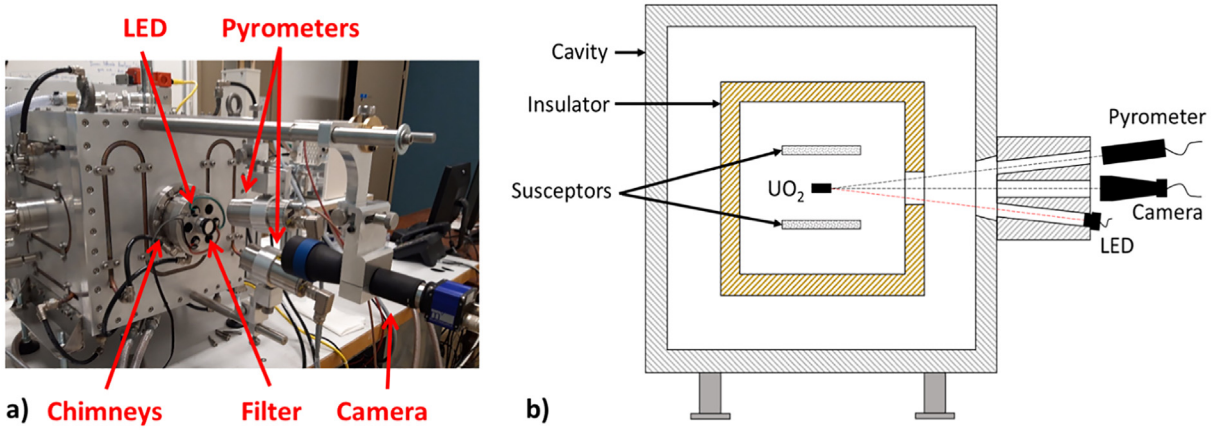

Fig. 3. a) Picture and b) drawing of devices (pyrometers, camera, filters and LEDs) and their arrangement for temperature and dilatometric measurements.

carried out for reproducibility. GeO_2 was used to determine ε for the monochromatic pyrometer and Nb_2O_5 enabled to calculate the emissivity ratio ($k = \varepsilon_1 / \varepsilon_2$) of the bichromatic pyrometer. Average values of 0.525 and 1 were determined for ε and k respectively.

2.3.3. Control of the thermal cycle

A specific control software was developed using Labview® to carry out sintering experiments with controlled heating cycles. This software uses a PID controller based on the temperature measured by pyrometers. The incident power delivered by the generator is continuously adjusted during the sintering cycle to match the measured temperature with the set temperature. Moreover, the impedance tuner is adjusted manually during heating to minimize the reflected power. The power sensors, the camera and the pyrometers are also connected to this Labview® software in order to record the data (power, temperature, images) used to control the thermal treatment and to obtain sintering curves (as conventional sintering in a dilatometer).

3. Experimental validation of the setup

Sintering tests were conducted using the developed microwave setup with the following two main targets:

- check the possibility to heat and sinter uranium oxide based samples in the cavity with the designed sintering cell,
- characterize the samples densification after sintering to demonstrate that equivalent characteristics of the pellets than under conventional heating can be obtained.

3.1. Preparation of samples and sintering parameters

UO_2 green pellets were prepared using uranium dioxide powder synthesized by the Ammonium Di-Uranate (ADU) process. The BET specific surface area of the powder is 3.02 $m^2.g^{-1}$. Cylindrical compacts were shaped by double-effect uniaxial cold pressing in a 10 mm diameter die at 350 MPa. To reduce the friction coefficient between the powder and the die and facilitate the compression, stearic acid was sprayed on the die surface. The density of the green bodies was around 5.8 g. cm^{-3}. The samples were inserted into the sintering cell described in part 2.2. Two types of plates (SiC and 3Y-TZP) were tested as susceptors inside the cell. The following thermal cycle was used: heating at a rate of 4 °C/min until 150 °C (for degassing and to avoid sample cracking) and then heating at a rate of 20 °C/min until 1650 °C with a dwell time of 10 min. After the dwell time, the microwave power was turned off for natural cooling. A flow and a slight overpressure of Ar/4%-H_2 was imposed in the cavity during the whole thermal cycle.

3.2. Sintering of UO_2 pellets: results and discussion

Fig. 4 presents the evolution of the recorded data (temperature, incident, absorbed and reflected power vs time) during heating of UO_2 pellets with SiC and 3Y-TZP susceptors (Fig. 4a and b).

Fig. 4a shows the data for hybrid heating of a UO_2 pellet with SiC susceptors. A constant heating rate of the UO_2 pellet of around 15 °C/min is measured until 1400 °C. From room temperature to 1400 °C, the PID controller increased constantly the incident power until 1400 W, to keep the heating rate of the pellet. It can be noticed that reflected power (outgoing from the cavity) is very low, all of the incident power is used by the pellet and susceptors. Above 1400 °C, an increase of the incident power is observed to keep a constant heating rate of the pellet. Strong variations of the incident power are also evidenced until 1586 °C, where heating was stopped due to the creation of unexpected gases and plasmas in the cavity. A visual control of susceptors and insulators after heating evidenced a change in the color of SiC plates and the presence of a yellow/brown deposit on thermal insulators.

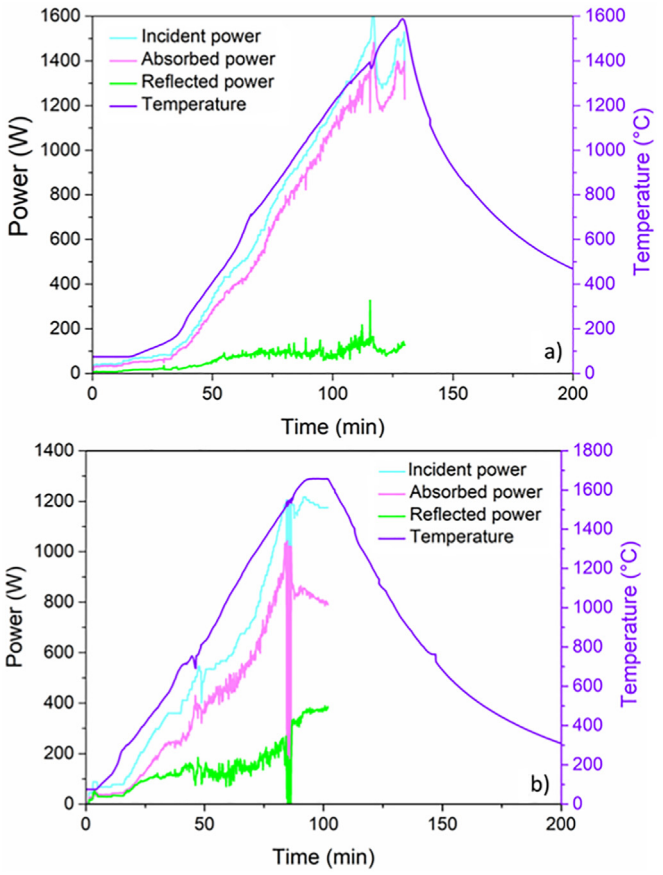

Fig. 4. Temperature and incident, absorbed and reflected powers vs time for the pellets sintered with a) SiC and b) 3Y-TZP susceptors.

Microscopic analysis (not shown here) showed a change in the morphology of SiC plates and XRD analysis demonstrated that the yellow/brown deposit was mainly composed of silicon. These analyses were explained by a reaction between SiC and H_2 above 1400 °C, leading to the creation of gaseous hydrides. This reaction explains the strong increase and variations of the incident power above 1400 °C (a part of the power was used to sustain reaction) and the difficulty to heat the pellet.

Fig. 4b shows the data for hybrid heating of a UO_2 sample with 3Y-TZP susceptors. A constant heating rate of the UO_2 pellet of 18.5 °C/min is measured until 1650 °C and the dwell time of 10 min was correctly followed. Only two small disturbances in the heating cycle can be observed. The first disturbance is located around 700 °C with a slight decrease of the pellet temperature, but quickly adjusted by the PID controller. This effect is due to the change in dielectric properties of 3Y-TZP susceptors around 700 °C. Indeed, the imaginary part of the 3Y-TZP permittivity quickly increases around 700 °C [25], leading to faster heating. The power inside the cavity was lowered to avoid thermal runaway of the susceptors, explaining the small decrease of the incident power and of the UO_2 pellet temperature around 700 °C, for a few tens of seconds. Afterwards, the PID controller adjusted progressively the incident power to follow the set thermal cycle. Optimization of the PID controller parameters will allow for a better control of this phenomenon. Automation of the impedance tuner is also planned to help minimizing the problem. The second disturbance can be observed between 1500 °C and 1600 °C. Fig. 5 presents a zoom on the temperature and incident power vs time curve for sintering with 3Y-TZP susceptors (Fig. 4b). This disturbance went along with important variations in the incident power sent to the cavity by the PID controller. This phenomenon can be attributed to the

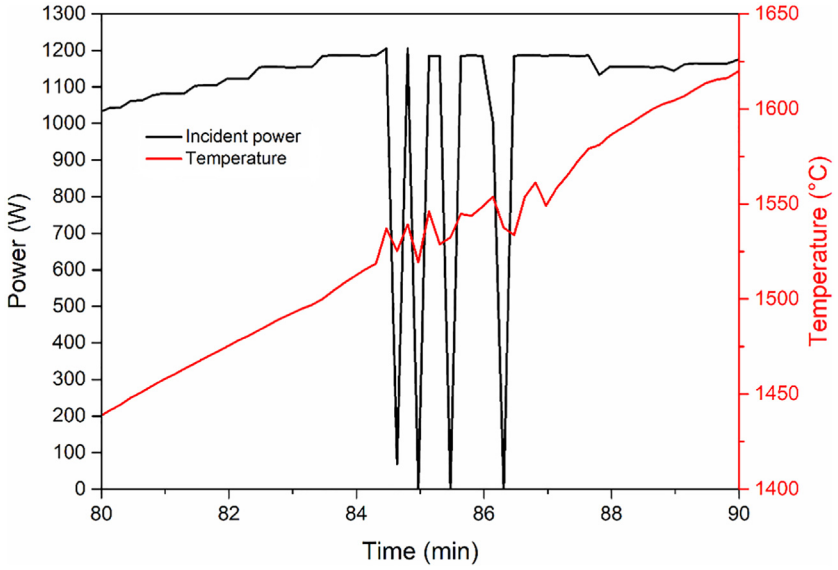

Fig. 5. Zoom on the temperature (black curve) and incident power (red curve) vs time curve (see Fig. 4b) for sintering with the 3Y-TZP susceptors in the range 1400–1650 °C.

increase of electrical conductivity of UO_2 [19] in this temperature range, which lead to a decrease of the electric field depth penetration inside the pellet. But, the increase of electrical conductivity was compensated by the increase of the dielectric loss of 3Y-TZP in this temperature range [24]. Therefore, as visible in Fig. 5, the disturbance lasted around 3 min and the follow-up of the set temperature took over just after, until 1650 °C.

Thermal images obtained with the bichromatic pyrometer were used to measure the temperature of a UO_2 pellet and its environment during microwave heating at 15 °C/min with 3Y-TZP susceptors (see Fig. 6). Fig. 6a shows that the pellet temperature is homogeneous but higher than its environment at low temperatures (under 1000 °C), due to the higher dielectric properties of UO_2 compared to 3Y-TZP susceptors (see Table 1). This image demonstrates that the designed sintering cell enables for hybrid heating of the UO_2 pellet. For higher temperatures, Fig. 6b and Fig. 6c show that the temperature of the pellet environment (sintering cell) increases because more power is dissipated in 3Y-TZP susceptors (change in their dielectric properties). The temperature of the cell and the pellet is equivalent for sintering temperatures (>1500 °C). The equivalent field distribution pattern inside both 3Y-TZP susceptors (see §2.2) induces equivalent heating of the lower and upper plate, which leads to homogeneous temperature inside the cell and the pellet (Fig. 6c). Although less energy is dissipated inside UO_2 at sintering temperatures due to the increase of its electrical conductivity (see §2.2) [19], thermal energy supplied by susceptors enables to keep a constant heating rate and homogeneous temperature of the pellet.

Fig. 4b also shows that the total power needed to heat the pellet until 1650 °C is 1200 W, lower than the power needed with SiC susceptor to heat only until 1400 °C (Fig. 4a). This is well correlated with FE simulation, which demonstrates a higher field intensity inside 3Y-TZP susceptors (see Table 2).

Carried out sintering experiments evidenced drawbacks for the use of SiC as susceptors. For the same thermal cycle, more power is needed with SiC than 3Y-TZP to heat the UO_2 pellet. However, more the power more the probability to create plasma or electrical arcs in the cavity under reducing atmosphere. Furthermore, reaction of SiC with H_2 above 1400 °C damages SiC plates, disturbs heating of the UO_2 pellet and pollutes the sintering cell and the sample.

These drawbacks prevent the use of SiC susceptors and only 3Y-TZP susceptors are suited for sintering of UO_2 pellets in the designed microwave setup.

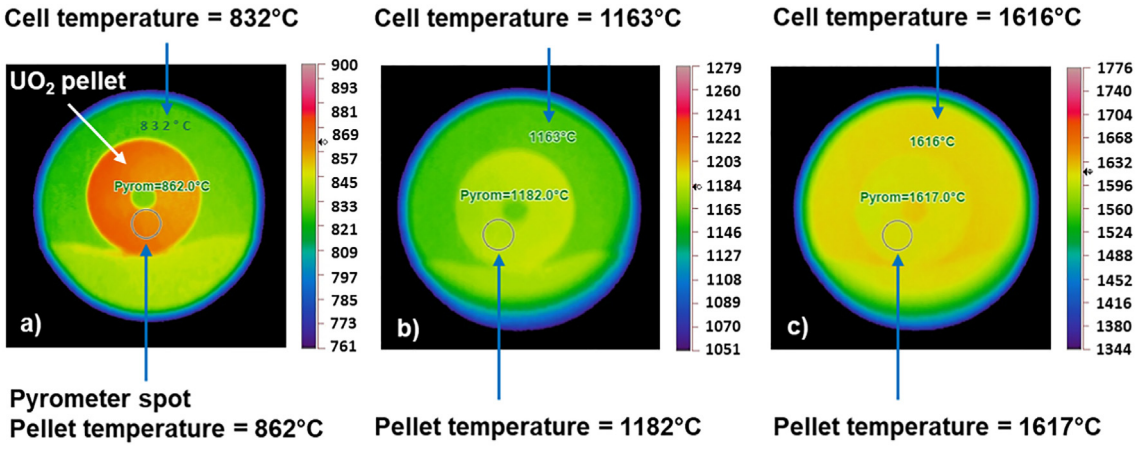

Fig. 6. Thermal images of a UO_2 pellet (annular shape) during microwave heating in the cell with 3Y-TZP susceptors at different pellet temperatures: a) 862 °C, b) 1182 °C and c) 1617 °C.

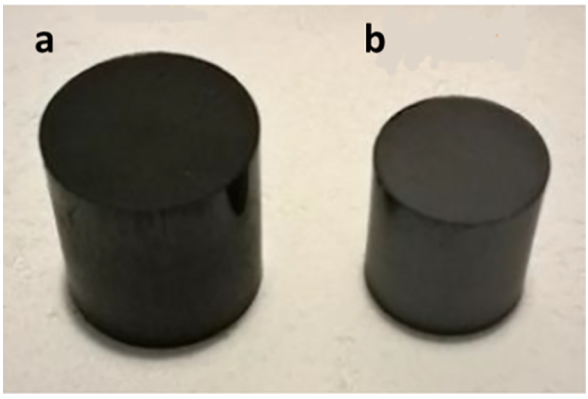

Fig. 7. Picture of a) green UO_2 pellet and b) UO_2 pellet sintered with 3Y-TZP susceptors.

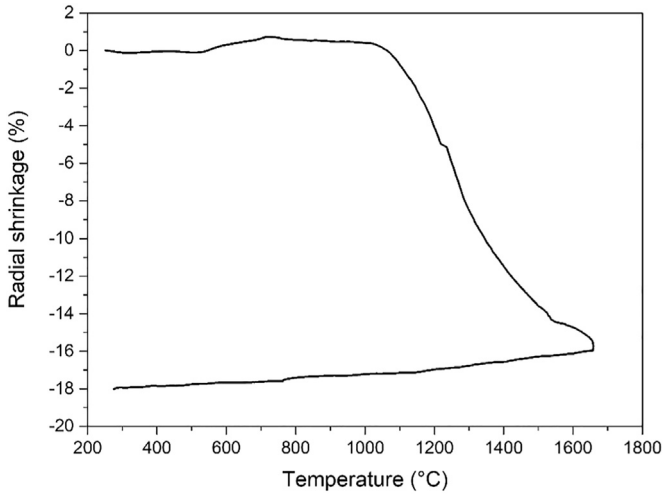

Fig. 8. Radial shrinkage vs temperature for the pellet sintered with 3Y-TZP susceptors at 1650 °C.

3.3. Densification of the samples

Fig. 7 presents pictures of a green UO_2 pellet and a UO_2 pellet sintered with 3Y-TZP susceptors. The sintered pellet is crack-free and the comparison with the green pellet shows the homogeneity of shrinkage. It demonstrates that heating of the pellet is homogeneous due to hybrid heating: pellets are heated in the bulk by direct interaction with microwaves and on their surface by radiation of the susceptor. Contrary to conventional sintering [18], high heating rates (>10 °C/min) can be used to sinter UO_2 pellets due to bulk heating, without leading to heterogeneous shrinkage. Moreover, no color change can be identified between green and sintered pellets (Fig. 7), assuming that no phase transformation from UO_2 to U_3O_8 or U_4O_9 phases have occurred during sintering: Ar/H_2 flow was appropriate to avoid detrimental oxidation [7]. These findings validate the use of the setup for homogeneous heating of UO_2 pellets until high temperatures (1650 °C) under reducing atmosphere, with controlled thermal cycles.

The final density of the pellet sintered with 3Y-TZP susceptors (Fig. 7b) was measured with the Archimedes method using ethanol as liquid medium. The pellet reached a final density of 10.2 $g.cm^{-3}$ (93% TD). This high density was obtained in a total sintering time of only 4 h, cooling comprised (see Fig. 5), although no particular optimization of the sintering parameters was performed. This density value is close to those obtained in conventional sintering with a total sintering time of 24 h and higher temperatures ([25–28]). The time needed to sinter UO_2 pellets with this innovative microwave sintering setup is divided by six compared to conventional sintering. The radial shrinkage of the pellet vs temperature, computed from the optical dilatometer and pyrometers data, is plotted in Fig. 8. A final radial shrinkage of −18% was reached. The accuracy of the optical dilatometer and the possibility to follow the shrinkage over time during microwave are demonstrated. The ability to calculate the instantaneous relative density for each temperature using radial shrinkage of the samples will be of high interest for future experiments. It will be possible to directly and reliably compare the sintering behavior of nuclear pellets under microwave heating and conventional heating.

4. Conclusion

The original instrumented and automated multimode cavity described in this paper allows reliable studies on the microwave sintering of nuclear ceramics under specific atmosphere. Dimensions of the cavity and the sintering cell were designed using FE simulation in order to perform hybrid microwave heating and to integrate the setup in a glovebox. The other originality of this setup is the use of a PID controller, coupled with an optical dilatometer and calibrated pyrometers, to control the heating rate and to measure the shrinkage of specimens. Recorded data during heating can be used for reliable comparison studies with conventional sintering behavior. These different elements of the setup are the main innovation of this work compared to previous studies on microwave sintering of nuclear ceramics in the literature. The first tests evidenced the possibility to control the heating of samples until high temperatures (1650 °C) under reducing atmosphere, without sparks or plasma. The homogeneous heating of the pellet is confirmed by thermal IR imaging during sintering. The first pellets of UO_2 sintered in the cavity reached 93%TD without deep optimization of the sintering parameters. This high density was obtained with a higher heating rate (20 °C/min) and thus, a shorter thermal cycle compared to conventional sintering. Therefore, this setup provides the opportunity for a more systematic sintering study of uranium oxide based nuclear materials (UO_2, $(U, Pu)O_2$, $(U, Am)O_2$ …) with the aim to obtain high densities in a considerably reduced sintering time compared to conventional sintering. Moreover, this setup will be used to study possible effects of microwaves on densification and microstructure of nuclear fuels.

Data availability

The raw/processed data required to reproduce these findings cannot be shared at this time due to legal or ethical reasons.

Declaration of Competing Interest

None.

Acknowledgements

This work was supported by the Commissariat à l'Energie Atomique et aux Energies Alternatives.

References

[1] K.I. Rybakov, E.A. Olevsky, E.V. Krikun, Microwave sintering: fundamentals and modeling, J. Am. Ceram. Soc. 96 (2013) 1003–1020, https://doi.org/10.1111/jace.12278.

[2] C. Singhal, Q. Murtaza, Parvej, microwave sintering of advanced composites materials: a review, Mater. Today Proc. 5 (2018) 24287–24298, https://doi.org/10.1016/j.matpr.2018.10.224.

[3] L. Gil-Flores, M.D. Salvador, F.L. Penaranda-Foix, A. Fernández, M. Suarez, R. Rosa, P. Veronesi, C. Leonelli, A. Borrell, Microstructure and mechanical properties of 5.8 GHz

microwave-sintered ZrO_2/Al_2O_3, Ceramics. Ceram. Int. 45 (2019) 18059–18064, https://doi.org/10.1016/j.ceramint.2019.06.026.
[4] P. Sikder, Y. Ren, S.B. Bhaduri, Microwave processing of calcium phosphate and magnesium phosphate based orthopedic bioceramics: a state-of-the-art review, Acta Biomater. 111 (2020) 29–53, https://doi.org/10.1016/j.actbio.2020.05.018.
[5] Y. Chen, B. Fan, B. Yang, W. Ma, G. Liu, H. Li, Microwave sintering and fracture behavior of zirconia ceramics, Ceram. Int. 45 (2019) 17675–17680, https://doi.org/10.1016/j.ceramint.2019.05.334.
[6] Y.V. Bykov, K.I. Rybakov, V.E. Semenov, High-temperature microwave processing of materials, J. Phys. D. Appl. Phys. 34 (2001) R55–R75, https://doi.org/10.1088/0022-3727/34/13/201.
[7] T.R.G. Kutty, P.V. Hegde, K.B. Khan, U. Basak, S.N. Pillai, A.K. Sengupta, G.C. Jain, S. Majumdar, H.S. Kamath, D.S.C. Purushotham, Densification behaviour of UO2 in six different atmospheres, J. Nucl. Mater. 305 (2002) 159–168, https://doi.org/10.1016/S0022-3115(02)00934-0.
[8] M. Le Guellec, F. Lebreton, L. Ramond, A. Ndiaye, T. Gervais, G. Bernard-Granger, Sintering investigations of a UO_2-PuO_2 powder synthesized using the freeze-granulation route, Scr. Mater. 186 (2020) 190–195.
[9] J.D. Ford, D.C.T. Pei, High temperature chemical processing via microwave absorption, J. Microw. Power. 2 (1967) 61–64, https://doi.org/10.1080/00222739.1967.11688647.
[10] T. Subramanian, P. Venkatesh, K. Nagarajan, P.R. Vasudeva Rao, A novel method of sintering UO_2 pellets by microwave heating, Mater. Lett. 46 (2000) 120–124, https://doi.org/10.1016/S0167-577X(00)00153-1.
[11] J.H. Yang, K.W. Song, Y.W. Lee, J.H. Kim, K.W. Kang, K.S. Kim, Y.H. Jung, Microwave process for sintering of uranium dioxide, J. Nucl. Mater. 325 (2004) 210–216, https://doi.org/10.1016/j.jnucmat.2003.12.003.
[12] S. Ramesh, N. Zulkifli, C.Y. Tan, Y.H. Wong, F. Tarlochan, S. Ramesh, W.D. Teng, I. Sopyan, L.T. Bang, A.A.D. Sarhan, Comparison between microwave and conventional sintering on the properties and microstructural evolution of tetragonal zirconia, Ceram. Int. 44 (2018) 8922–8927, https://doi.org/10.1016/j.ceramint.2018.02.086.
[13] S. Vijayan, H. Varma, Microwave sintering of nanosized hydroxyapatite powder compacts, Mater. Lett. 56 (2002) 827–831, https://doi.org/10.1016/S0167-577X(02)00622-5.
[14] E. Pert, Y. Carmel, A. Birnboim, T. Olorunyolemi, D. Gershon, J. Calame, I.K. Lloyd, O.C. Wilson, Temperature measurements during microwave processing: the significance of thermocouple effects, J. Am. Ceram. Soc. 84 (2001) 1981–1986, https://doi.org/10.1111/j.1151-2916.2001.tb00946.x.
[15] D. Żymełka, S. Saunier, J. Molimard, D. Goeuriot, Contactless monitoring of shrinkage and temperature distribution during hybrid microwave sintering, Adv. Eng. Mater. 13 (2011) 901–905, https://doi.org/10.1002/adem.201000354.
[16] J. Croquesel, D. Bouvard, J.-M. Chaix, C.P. Carry, S. Saunier, Development of an instrumented and automated single mode cavity for ceramic microwave sintering: application to an alpha pure alumina powder, Mater. Des. 88 (2015) 98–105, https://doi.org/10.1016/j.matdes.2015.08.122.
[17] R. Heuguet, S. Marinel, A. Thuault, A. Badev, Effects of the susceptor dielectric properties on the microwave sintering of alumina, J. Am. Ceram. Soc. 96 (2013) 3728–3736, https://doi.org/10.1111/jace.12623.
[18] D. Żymełka, S. Saunier, D. Goeuriot, J. Molimard, Densification and thermal gradient evolution of alumina during microwave sintering at 2.45GHz, Ceram. Int. 39 (2013) 3269–3277, https://doi.org/10.1016/j.ceramint.2012.10.015.
[19] J.L. Bates, C.A. Hinman, T. Kawada, Electrical conductivity of uranium dioxide, J. Am. Ceram. Soc. 50 (1967) 652–656, https://doi.org/10.1111/j.1151-2916.1967.tb15021.x.
[20] R.R. Mishra, A.K. Sharma, Microwave–material interaction phenomena: heating mechanisms, challenges and opportunities in material processing, Compos. A: App. Sci. Manuf. 81 (2016) 78–97.
[21] K. Gesi, J. Tateno, Dielectric constant of UO2 at 9.4 GHz, Jpn. J. Appl. Phys. 8 (1969) 1358, https://doi.org/10.1143/JJAP.8.1358.
[22] C. Manière, T. Zahrah, E.A. Olevsky, Fully coupled electromagnetic-thermal-mechanical comparative simulation of direct vs hybrid microwave sintering of 3Y-ZrO_2, J. Am. Ceram. Soc. 100 (2017) 2439–2450.
[23] R. Macaigne, S. Marinel, D. Goeuriot, C. Meunier, S. Saunier, G. Riquet, Microwave sintering of pure and TiO_2 doped $MgAl_2O_4$ ceramic using calibrated, contactless in-situ dilatometry, Ceram. Int. 42 (2016) 16997–17003, https://doi.org/10.1016/j.ceramint.2016.07.206.
[24] M. Arai, J.G.P. Binner, T.E. Cross, Comparison of techniques for measuring high-temperature microwave complex permittivity: measurements on an alumina/Zircona system, J. Microw. Power Electromagn. Energy. 31 (1996) 12–18, https://doi.org/10.1080/08327823.1996.11688287.
[25] K.W. Song, K. Sik Kim, K. Won Kang, Y. Ho Jung, Grain size control of UO_2 pellets by adding heat-treated U3O8 particles to UO2 powder, J. Nucl. Mater. 317 (2003) 204–211, https://doi.org/10.1016/S0022-3115(03)00080-1.
[26] K.C. Radford, R.J. Bratton, Properties, blending and homogenization of (U, Th)O_2-UO_2 powder, J. Nucl. Mater. 57 (1975) 287–302, https://doi.org/10.1016/0022-3115(75)90213-5.
[27] Y. Harada, UO_2 sintering in controlled oxygen atmospheres of three-stage process, J. Nucl. Mater. 245 (1997) 217–223, https://doi.org/10.1016/S0022-3115(96)00755-6.
[28] D.S. Kumar, K. Ananthasivan, A. Dasgupta, Low temperature two-step sintering of nanocrystalline UO_2, J. Nucl. Mater. 510 (2018) 131–140, https://doi.org/10.1016/j.jnucmat.2018.07.033.